RESEARCH ARTICLE

CLOUDS

Locally narrow droplet size distributions are ubiquitous in stratocumulus clouds

Nithin Allwayin[1], Michael L. Larsen[1,2]*, Susanne Glienke[3], Raymond A. Shaw[1]*

Marine stratocumulus clouds are the "global reflectors," sharply contrasting with the underlying dark ocean surface and exerting a net cooling on Earth's climate. The magnitude of this cooling remains uncertain in part owing to the averaged representation of microphysical processes, such as the droplet-to-drizzle transition in global climate models (GCMs). Current GCMs parameterize cloud droplet size distributions as broad, cloud-averaged gammas. Using digital holographic measurements of discrete stratocumulus cloud volumes, we found cloud droplet size distributions to be narrower at the centimeter scale, never resembling the cloud average. These local distributions tended to form pockets of similar-looking cloud regions, each characterized by a size distribution shape that is diluted to varying degrees. These observations open the way for new modeling representations of microphysical processes.

Earth's radiation and water balances depend strongly on cloud properties, and their calculation in global climate models (GCMs) relies on the assumed cloud droplet size distribution structure (*1*, *2*). These droplet size distributions are based on spatially averaged measurements of cloud droplet number concentration and diameter (*3*) and are often represented as modified gamma distributions (*4*, *5*). The use of cloud-averaged distribution shapes implies that cloud processes and interactions at droplet scales are only approximately captured (*6*–*8*) and contributes prominently to uncertainties in GCM response to perturbations (*9*). For example, calculations of drizzle formation rate must be corrected to account for spatial correlations in droplet number concentration N owing to a nonlinear dependence that scales as N^2 (*10*) and spatial correlations between N and cloud liquid water mixing ratio q_c (*11*–*13*). Additionally, changes in size distribution shape are also dramatically important for drop collision characterization owing to a drop diameter–dependent D^6 scaling (*14*). Although the dependence of cloud size distribution shape on spatial averaging scales has been extensively explored (*15*, *16*), limited spatial resolution in models has hindered the quantification of microphysically relevant "local" size distributions. In this work, we used cloud measurements made with a digital holographic cloud imaging instrument (Holographic Detector for Clouds, HOLODEC) (*17*–*20*) to obtain locally sampled cloud droplet size distributions in ~10-cm^3 volumes at regular intervals as a plane traverses through a cloud. This approach contrasts with the typical ~10- to 100-m averaging scale for airborne measurements of droplet size distributions. Fine-scale measurements of liquid water content (LWC) have been made (*21*), but they do not explore the structure of the droplet size distribution, and they break down in the presence of large-scale drops common in stratocumulus clouds (*22*). By then using a machine-learning algorithm based on hypothesis testing (*23*), we investigated whether the gamma-type representations of cloud droplet size distributions used in GCMs hold for these much smaller and microphysically relevant spatial scales. This measurement strategy allowed us to ask several fundamental questions relevant to the microphysical and optical properties in clouds: Do local cloud droplet size distributions look like the broad, cloud-averaged values? If not, what distribution shapes occur, and are those shapes correlated or isolated in space? Are local size distribution shape, droplet concentration, and other variables related in a simple way?

The analysis was performed on HOLODEC data from low-level marine stratocumulus clouds near the Azores islands in the Atlantic Ocean during the Aerosol and Cloud Experiments in the Eastern North Atlantic (ACE-ENA) field campaign (*24*, *25*). The ACE-ENA campaign had the objective of better characterizing the marine low-level clouds and associated aerosol and atmospheric boundary layer properties. These stratocumulus clouds are radiatively extremely important and are composed of individual convective elements combining to form a corrugated, carpet-like appearance (*26*). They are thin clouds with a vertical extent of a few hundred meters, usually residing in the bottom couple of kilometers of the atmosphere. A stratocumulus cloud system is typically assumed to be homogeneous within a grid [illegible] of a coarse-resolution cloud model; this [illegible] homogeneity, or lack thereof, is a central aspect of this study.

We investigated data from horizontal cloud transects at constant altitudes and over length scales that approached the typical grid box length scales of GCMs for four flights in the ACE- ENA field project, covering a range of cloud conditions (tables S1 and S2). Each of the cloud transects was designed to sample clouds at a constant altitude in an "L" shape before moving to a different altitude. This would suggest that any differences in droplet size distributions are not from differences in adiabatic growth profiles at different heights (assuming a constant cloud base), thus helping to isolate the horizontal inhomogeneity.

In a given flight segment, the size distributions in all holograms of a truly well-mixed, homogeneous cloud would be similar to each other, with only slight differences due to sampling. Presumably, these distributions would all appear similar to the cloud-averaged gamma distributions typically observed and used in models and remote sensing retrievals. Alternatively, in another extreme limit, it is possible that even well-mixed stratocumulus clouds remain microphysically heterogeneous with each holographic volume, revealing disparate local droplet size distributions with no two volumes in the cloud resembling each other.

What we needed was a way to explore how measured droplet size distributions vary and how they compare to each other. When we first started this investigation, we asked the simple question: Do local droplet size distributions look like the mean for a flight segment? The answer was almost universally no. That inspired a related question: Do local size distributions ever look like each other? As a result, we developed the algorithm described by Allwayin *et al.* (*23*), designed to compare individual local droplet size distributions and group them into clusters of distributions with similar shapes. This is achieved by combining a nonparametric hypothesis test that identifies the holograms having the same distribution shapes with a clustering algorithm that groups these similar holograms. No assumption about the functional form of the underlying distribution shapes is used in the algorithm (see the supplementary materials for more details on the algorithm). For a given segment, the algorithm outputs groups of holograms that have the same underlying distribution shape. Each such group can therefore be represented by a single distribution shape, referred to in this work as the characteristic droplet size distribution. A relatively small number of such characteristic distributions holds the potential to encapsulate spatial variabilities in cloud microphysical properties along a horizontal flight path.

[1]Department of Physics, Michigan Technological University, Houghton, MI 49931, USA. [2]Department of Physics and Astronomy, College of Charleston, Charleston, SC 29424, USA. [3]Atmospheric, Climate, and Earth Sciences Division, Pacific Northwest National Laboratory, Richland, WA 99354, USA.
*Corresponding author. Email: larsenml@cofc.edu (M.L.L.); rashaw@mtu.edu (R.A.S.)

Each of these local size distributions could potentially appear anywhere within the flight segment, but we show below that it is common for holograms in the same "cluster" to appear spatially near each other in the cloud. Notably, none of these clusters have the shape of the cloud-averaged size distribution; the clusters exhibit relatively narrow size distributions that, when averaged over a cloud, combine to construct the assumed broad shape used in GCMs.

Results and discussion

In an overwhelming majority (30 out of 31) of the cloud transects analyzed, multiple local characteristic size distribution shapes were identified. Characteristic size distributions were thus found to be ubiquitous and to exist for segments across multiple research flights spanning a variety of cloud conditions. This suggests that the global cloud size distribution formed by combining all droplets in a given cloud segment can be decomposed into multiple characteristic distributions. These characteristic distributions were formed by local cloud samples of nearly identical size distribution shapes and were identified by the algorithm as clusters, an example of which is illustrated in Fig. 1. The cloud transect shown is for a 60-km segment at an altitude of 850 m, obtained during the research flight on 18 July 2017. The distributions were normalized as probability density functions (PDFs), and a cluster only depended on the shapes of the individual size distributions, each with an assigned line color (Fig. 1A). Additionally, not all local samples were classified with a cluster, as shown by the unclustered light gray distributions. The relative frequency of occurrence can be seen in the cloud droplet number-size distributions (Fig. 1B). The average size distribution formed by combining the cloud drops from all holograms is shown by the thick black line. It is clearly evident that the individual, local cloud size distributions are narrow when compared with the segment-averaged global distribution and have peaks spanning a range of diameters (Fig. 1B). They have almost no similarity in appearance to the global averaged distribution, and indeed, nearly all individual holograms failed the Kolmogorov-Smirnov hypothesis test for statistical similarity (fig. S1). This holds in general for all the other flight segments analyzed as well. For most cases, the local characteristic distributions were narrow and did not match the averaged distribution, typically with <10% of the holograms looking like the segment-averaged value (tables S1 and S2). Further, the weighted combination of all the characteristic local distributions gave rise to a gamma-like distribution that is broader and has a long large-drop tail. The local-versus-global distribution properties for the segment shown previously are compared in Fig. 2, where distribution spreads

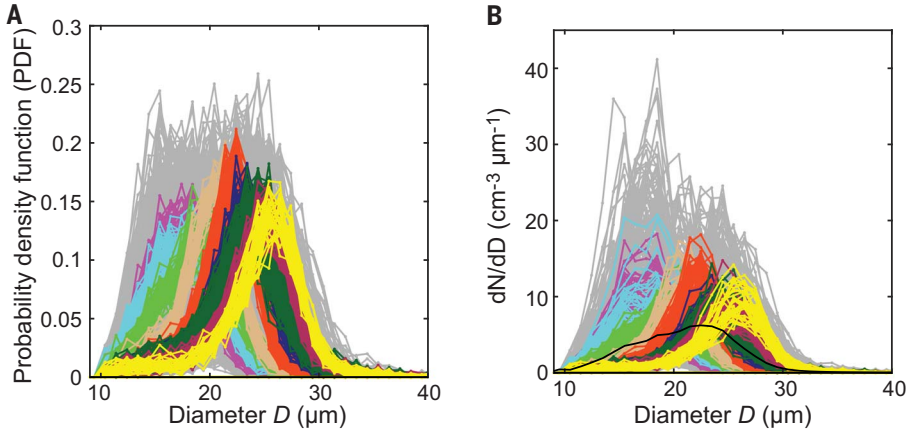

Fig. 1. Characteristic distributions identified by the algorithm for centimeter-scale local droplet size distributions measured with HOLODEC. Clusters of identical-looking local cloud volumes given by (**A**) the PDFs and (**B**) the bin width–normalized number-size distributions (dN/dD) of all cloud holograms for a 60-km flight segment from the ACE-ENA research flight on 18 July 2017 at an altitude of 850 m. The different colors denote the individual clusters, and the gray lines indicate identify holograms not classified into a cluster. The solid black line in (B) represents the global average distribution of the segment. The local cloud droplet size distributions are narrow when compared with the segment-averaged global distribution and have peaks spanning a range of diameters. The distributions have a lower size resolution of 10 μm, and a bin width of 1 μm was used for the figure (though the algorithm determined the classifications by using raw, unbinned data).

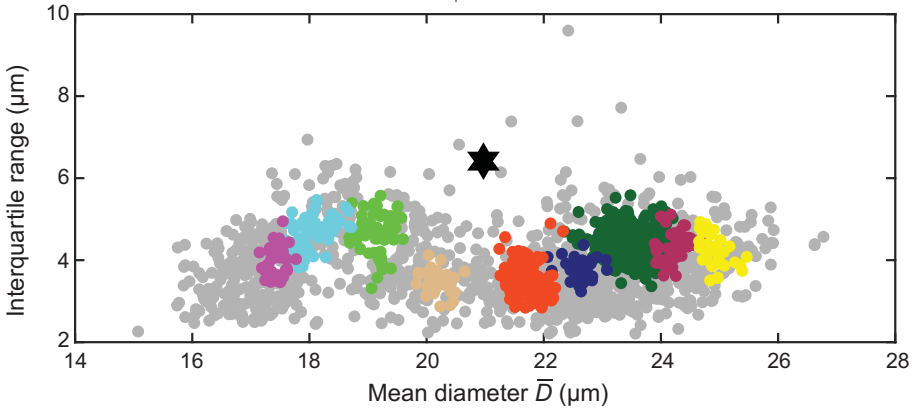

Fig. 2. Comparison of the local versus global distribution properties. A measure of the width of local distribution, the interquartile range, versus the mean diameter is shown. Individual holograms are shown as circles, with clusters denoted by the same color scheme as used in Fig. 1. The black star indicates the segment average, and the gray circles indicate the unclassified holograms. The local distributions bear little resemblance to the global average, suggesting that the global mean and width of the droplet size distributions are not representative of cloud structures at small scales. All holograms are from the same segment as in Fig. 1, a 60-km flight segment on 18 July 2017 at an altitude of 850 m.

are given by the interquartile ranges of particle diameters for individual hologram samples versus mean droplet diameter. The global distribution properties are denoted by the star (Fig. 2). Almost all of the hologram distributions bear little resemblance to the global average, suggesting that the global mean and width of the droplet size distributions are not representative of cloud structures at small scales. This is true even for the corresponding holograms not belonging to any identified size-distribution archetype but still conveying information about local drop distributions (gray circles, Fig. 2). The observed narrowness of the local size distributions naturally leads to questions about the nature and extent of turbulent mixing in stratocumulus clouds. A characteristic distribution shape may suggest similar microphysical histories that persist without fully mixing with the rest of the cloud by turbulence.

Do the clusters of common distribution shapes tend to reside near each other in space? As illustrated in Fig. 3, these characteristic distribution clusters tend to occur in blocks of

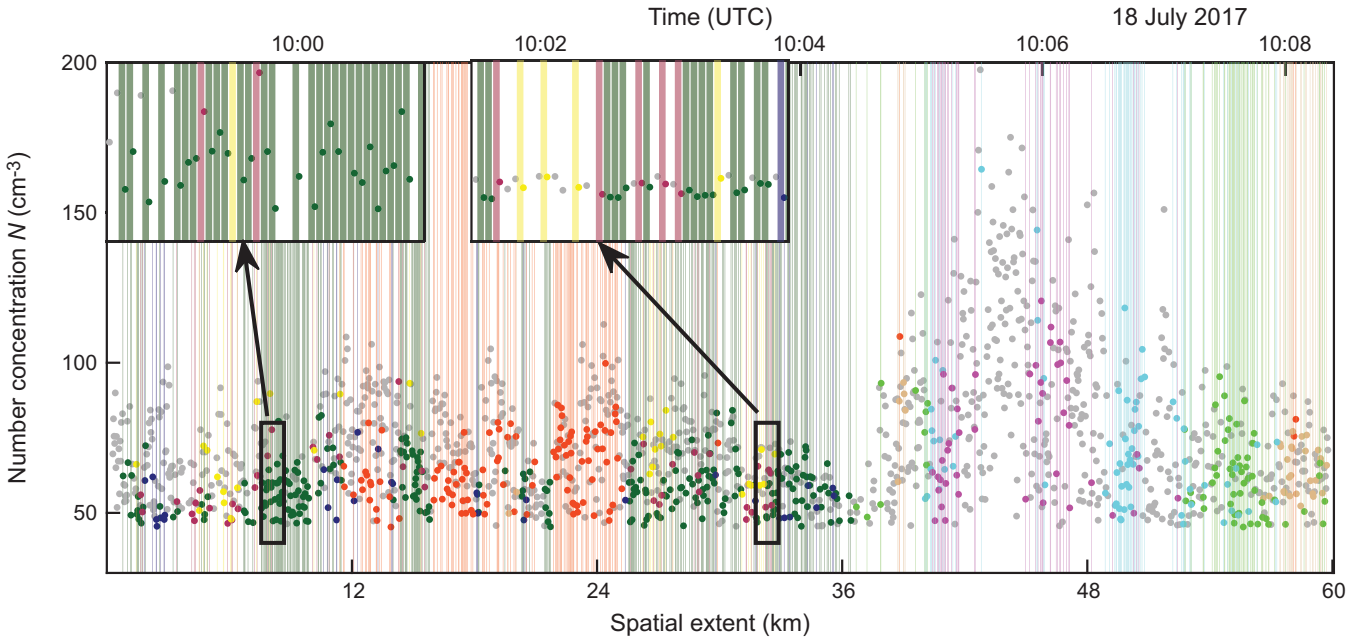

Fig. 3. Spatial structure of the local characteristic distributions. The spatial-temporal evolution of hologram number concentrations demonstrates that like-classified local cloud regions occur in small blocks of successive holograms. Bar colors identify the same clusters as shown in Figs. 1 and 2. These blocks vary in spatial extent and are sometimes separated by kilometers. These blocks do not have sharp boundaries and contain different cluster types, as shown by the zoomed-in views from the inset plots. Each slice for the inset plot is 12 s long, corresponding to about 1.2 km. Gaps correspond to holograms that were not put into any cluster by the classification algorithm.

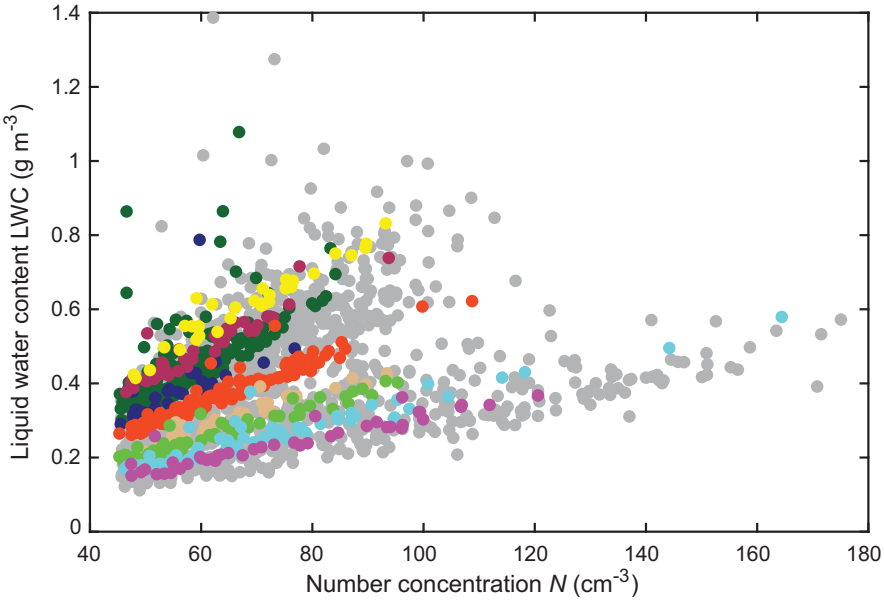

Fig. 4. Cloud LWC versus cloud droplet concentration, suggesting that microphysical relationships for individual clusters of similar holograms can reflect cloud histories. Cloud LWC and number concentrations for different clusters have a linear relationship, with slope depending on the cluster type. As the distribution shape and, correspondingly, the mean diameter remain constant for holograms of a cluster, the linear reduction in LWC with number concentration suggests a predominance of dilution and, complete evaporation of droplets during the mixing process with dry environmental air (inhomogeneous mixing). The separate clusters are denoted by the different colors, as defined in Figs. 1 and 2, with gray dots representing the unclassified holograms.

successive holograms varying in spatial extent. Nevertheless, spatial correlation between cluster members is not absolutely universal, and a characteristic distribution is not confined to just one region of the cloud, with most of these clusters appearing in multiple blocks spatially separated often by many kilometers. These blocks do not have hard boundaries and can have members from other clusters embedded within them (insets, Fig. 3). The block-like clustering behavior implies that "similar-looking" holograms do not appear at random but rather appear in zones with similar microphysical properties. Note that the algorithm has a few adjustable parameters that can fine-tune the properties of these clusters. Notably, however, the qualitative features of these results are practically always preserved.

The results unequivocally demonstrate the existence of local-scale characteristic distributions in stratocumulus cloud systems. These distributions are narrower, with distinguishable modes, and differ considerably from the global averaged distributions. The differences between the characteristic distributions can reveal important information about cloud microphysical properties previously undiscernible

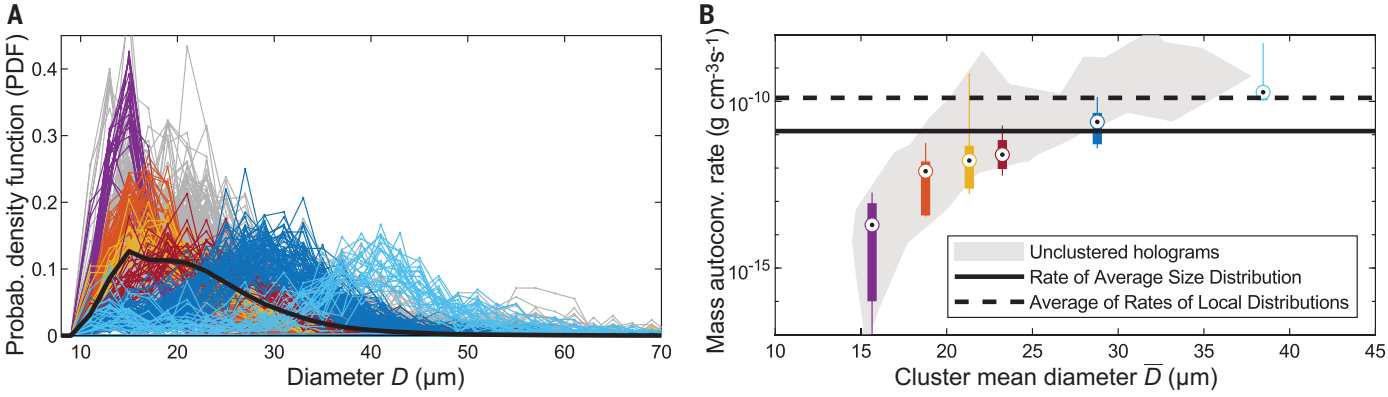

Fig. 5. Collisional growth rates for characteristic droplet size distributions. The mass autoconversion rate is a measure of initial cloud droplet growth by collision-coalescence until efficient development of precipitation by accretion. (**A**) The different colors correspond to the characteristic distributions, and the gray marks the unclustered holograms. The solid black line represents the global distribution for the entire segment. (**B**) Mass autoconversion rates for the different characteristic distributions versus the mean diameter of the local distributions. The box plots display the median (central dot), the 25th and 75th percentiles (box), and the 5th and 95th percentiles (lines) of the local autoconversion rates for the holograms in each cluster, with the color scheme the same as in (A). Most of the individual process rates differ substantially from the value calculated with the average size distribution, which is represented by the solid black line. That global average rate also differs by an order of magnitude from the average of the local autoconversion rates, which is shown by the dashed black line. The gray region marks the range of autoconversion rates for the unclustered holograms. The data are from a 40-km flight segment in a stratocumulus cloud on 19 July 2017 at an altitude of 1350 m.

from a global averaged representation and thus help improve cloud representations for models. Figure 4 demonstrates the relationship between the cloud LWC and droplet number concentration N for individual cloud samples. Again, characteristic size distributions are shown by the colored dots. The covariance between liquid water content and particle number concentration can have direct implications for autoconversion rates (*12*, *13*) used in cloud models. Universally for all flight segments analyzed, the characteristic distributions tend to fall along straight lines with differing slopes. As the distribution shape for a cluster of holograms is identical, the decrease in LWC with a reduction in number concentration is a signature of inhomogeneous mixing (*20*, *27*–*29*), i.e., the evaporation of a subset of droplets during the mixing of a cloud parcel with dry environmental air. These clusters could then be interpreted as resulting from a finite set of different parcels within a region with initially similar and narrow size distribution, each of which have been inhomogeneously mixed to varying degrees (*30*). An assumption of cloud-environment mixing primarily composed of inhomogeneous mixing events substantially simplifies radiative calculations in dual-moment bulk microphysical schemes in widely used coarse-resolution models (*31*). This inhomogeneous-mixing signature is not simply the result of the algorithm used; it is not self-evident that only narrow, rather than broad distributions should exist, and it is also not obvious that narrow distributions with a certain mean diameter should exist with a wide range of droplet concentrations. By contrast, some implementations of gamma-distributed cloud droplet size distributions assume a dependence of the standard deviation on the number concentration.

These characteristic distributions were ubiquitously observed for a variety of cloud and boundary layer conditions, and although this very universality is striking, it makes it difficult to isolate the physics behind their existence. One hypothesis to partly explain the differences across various clusters may be spatial variability of cloud condensation nuclei concentrations in the boundary layer (*32*). For the same LWC, differences in number concentrations can result in characteristic distributions with different mode diameters. Differences in lifting condensation levels (LCL) within the boundary layer, resulting from previous large-scale entrainment events, could be another mechanism contributing to the formation of these clusters (*33*). The resulting differences in cloud depths and the associated adiabatic growth profiles can show up as clusters of different modes (*34*). LCL variability is also linked to mesoscale organization. Variations in surface fluxes and decoupling strength also affect the variability of the LCL (*35*) and thereby explain the characteristic distributions. Entrainment mixing of dry environmental air and the associated microphysical and dynamical response may be another explanation for these results. Vertical circulation mixing after entrainment events could result in local distributions with a range of diameters even at constant altitudes (*34*), and these entrainment regions have length scales similar to the observed characteristic distributions (*36*). More research is required to quantify and fully unravel the nature and physics of these regions defined by characteristic distributions.

The results presented in this work have implications for precipitation formation and its treatment in numerical models. Autoconversion represents the collision of small cloud droplets starting the rain formation process (*1*). Precipitation initiation depends on local-scale cloud properties; the observation that cloud droplet size distributions at these scales do not match the cloud average value has an overarching significance for calculations of autoconversion rates. In Fig. 5, we show characteristic droplet size distributions from another stratocumulus cloud (40-km horizontal flight segment from 19 July 2017) together with calculated autoconversion rates to highlight the consequences of such local-scale variability. The left panel shows the six characteristic distributions that were identified by the algorithm (Fig. 5A). As in the case discussed previously, most local distributions did not resemble the gamma-like global cloud-averaged size distribution shape shown by the black line. The box plots in Fig. 5B display the mass autoconversion rates calculated for holograms of each characteristic distribution. The rate is a function of the cloud LWC and droplet number concentration, but significant for this work, it also depends on the shape of the droplet size distribution (*37*) (see the supplementary materials for details regarding the calculation). Most of the cloud had autoconversion rates that significantly differed from that calculated with the average size distribution (black line), with the local rates spanning a range of over five orders of magnitude.

Notably, even an average of all the local rates (dashed black line) differed from the global rate calculated from the size distribution of all cloud drops in the segment by an order of magnitude (which we might expect owing to Jensen's inequality). A calculation based on the cloud-averaged size distribution would consequently be biased. The magnitude of these differences depends on the nature of the local characteristic distributions and hence varies for the other cloud segments (see supplementary materials). Adequate estimation of the local autoconversion rate not only requires a measure of local number concentration and LWC but also an accounting for the local distribution shape.

The varying mean droplet diameters found in different characteristic distributions also have implications for estimates of cloud microphysical properties from remote sensing retrievals. Horizontal variability in cloud effective radius, LWC, and corresponding optical thickness are known to contribute substantially to biases of microphysical retrievals from satellite measurements (*38*, *39*). Analogous to the autoconversion rate calculations presented above, reflectances for local distributions will be different from the average reflectance computed from the full-cloud size distribution. New satellite instruments based on polarimetry (e.g., NASA's Atmosphere Observing System mission) are sensitive to the cloud-top region, and therefore, the existence of local size distributions may need to be accounted for.

The observation that characteristic droplet size distributions from individual 10-cm–scale holographic sample volumes tend to appear in regions with length scales spanning tens of kilometers provides support for the use of more-common cloud droplet instruments that average over 10- to 100-m length scales in future investigations of characteristic distributions within stratocumulus clouds. Measurements made in different stratocumulus cloud environments, e.g., with different levels of entrainment or surface coupling, can then guide the development of parameterizations of subgrid-scale variability for coarse-resolution models. For example, the results have implications for how to address the implicit dependence of distribution width on distribution moments, such as effective radius or liquid water content, i.e., the dispersion effect (*40*). Our findings can also guide the development of new approaches that are already underway, such as three-moment bulk representation of clouds in GCMs with distribution shape considered as a third prognostic variable (*41*). Specifically, the observations quantify the variability in distribution shape and the associated length scales related to size distribution changes.

Digital holographic imaging of droplets contained in localized volumes of ~10 cm^3 within stratocumulus clouds revealed that droplet size distributions at the local microphysics 10-cm scale are narrow compared with the average size distribution. Using distribution-independent hypothesis testing and machine-learning data clustering, we classified clusters of "characteristic" size distributions. The clusters tended to be spatially correlated on kilometer length scales. Furthermore, narrow characteristic distributions appeared with a wide range of droplet concentrations within those regions, consistent with expectations for inhomogeneous mixing caused by cloud-top entrainment. The broad gamma-like distributions often used in climate models and satellite retrievals were only achieved when averaging >10-km length scales. Local cloud droplet collision rates, calculated from mass autoconversion rates for the characteristic size distributions, varied by orders of magnitude. Furthermore, most local autoconversion rates differed substantially from the autoconversion rate calculated with the global average size distribution, and for the flight segment presented in this work, the average of local autoconversion rates differed from the autoconversion rate of the average distribution by about an order of magnitude. This helps to illustrate the importance of accounting for subgrid-scale fluctuations in number concentration, LWC, and size-distribution shape.

One could say that droplets in stratocumulus clouds are parochial, tending to live in their own spatial blocks of similar-looking, narrow size distributions. The local droplet concentrations can be diluted to varying degrees, but the distribution shapes tend to persist in these blocks. This has implications for microphysical process rates, which depend on local rather than global distribution properties. To turn the common phrase "all politics is local," we might say that all microphysics is local.

REFERENCES AND NOTES

1. Y. Liu, P. H. Daum, *J. Atmos. Sci.* **61**, 1539–1548 (2004).
2. G. L. Stephens *et al.*, *J. Geophys. Res.* **115** (D24), D24211 (2010).
3. N. L. Miles, J. Verlinde, E. E. Clothiaux, *J. Atmos. Sci.* **57**, 295–311 (2000).
4. J. E. Hansen, L. D. Travis, *Space Sci. Rev.* **16**, 527–610 (1974).
5. F. Tampieri, C. Tomasi, *Tellus Ser. A, Dyn. Meterol. Oceanogr.* **28**, 333–347 (1976).
6. D. Randall, M. Khairoutdinov, A. Arakawa, W. Grabowski, *Bull. Am. Meteorol. Soc.* **84**, 1547–1564 (2003).
7. W. W. Grabowski *et al.*, *Bull. Am. Meteorol. Soc.* **100**, 655–672 (2019).
8. H. Morrison *et al.*, *J. Adv. Model. Earth Syst.* **12**, MS001689 (2020).
9. D. Konsta *et al.*, *Geophys. Res. Lett.* **49**, e2021GL097593 (2022).
10. R. A. Shaw, *Annu. Rev. Fluid Mech.* **35**, 183–227 (2003).
11. Z. Zhang *et al.*, *Atmos. Chem. Phys.* **19**, 1077–1096 (2019).
12. Z. Zhang *et al.*, *Atmos. Chem. Phys.* **21**, 3103–3121 (2021).
13. J. A. Covert, D. B. Mechem, Z. Zhang, *Atmos. Chem. Phys.* **22**, 1159–1174 (2022).
14. A. B. Long, *J. Atmos. Sci.* **31**, 1040–1052 (1974).
15. Y. Liu, J. Hallett, *J. Atmos. Sci.* **55**, 527–536 (1998).
16. Y. Liu, P. H. Daum, J. Hallett, *J. Atmos. Sci.* **59**, 2279–2290 (2002).
17. J. P. Fugal, R. A. Shaw, E. W. Saw, A. V. Sergeyev, *Appl. Opt.* **43**, 5987–5995 (2004).
18. J. Fugal, R. Shaw, *Atmos. Meas. Tech.* **2**, 259–271 (2009).
19. S. M. Spuler, J. Fugal, *Appl. Opt.* **50**, 1405–1412 (2011).
20. M. J. Beals *et al.*, *Science* **350**, 87–90 (2015).
21. A. B. Davis, A. Marshak, H. Gerber, W. J. Wiscombe, *J. Geophys. Res.* **104** (D6), 6123–6144 (1999).
22. M. Wendisch, T. J. Garrett, J. W. Strapp, *J. Atmos. Ocean. Technol.* **19**, 1577–1584 (2002).
23. N. Allwayin, M. L. Larsen, A. G. Shaw, R. A. Shaw, *Artif. Intell. Earth Syst.* **1**, e220003 (2022).
24. J. Wang *et al.*, *Bull. Am. Meteorol. Soc.* **103**, E619–E641 (2022).
25. R. Shaw, Holographic Detector for Clouds (HOLODEC) droplet size distributions, Atmospheric Radiation Measurement (ARM) Archive (2018); https://doi.org/10.5439/1617265.
26. R. Wood, *Mon. Weather Rev.* **140**, 2373–2423 (2012).
27. M. B. Baker, R. G. Corbin, J. Latham, *Q. J. R. Meteorol. Soc.* **106**, 581–598 (1980).
28. K. Lehmann, H. Siebert, R. A. Shaw, *J. Atmos. Sci.* **66**, 3641–3659 (2009).
29. C. Lu, Y. Liu, S. Niu, S. Endo, *J. Geophys. Res. Atmos.* **119**, 13,877–13,890 (2014).
30. S. S. Yum *et al.*, *J. Geophys. Res. Atmos.* **120**, 5047–5069 (2015).
31. K. J. Sanchez *et al.*, *Atmos. Chem. Phys.* **17**, 9797–9814 (2017).
32. X. Zheng *et al.*, *Adv. Atmos. Sci.* **39**, 2107–2123 (2022).
33. J. Wang *et al.*, *J. Geophys. Res.* **114**, D18210 (2009).
34. F. Yang, R. Shaw, H. Xue, *Atmos. Chem. Phys.* **16**, 9421–9433 (2016).
35. X. Zhou, C. S. Bretherton, *J. Adv. Model. Earth Syst.* **11**, 3–18 (2019).
36. J. Yeom *et al.*, *Q. J. R. Meteorol. Soc.* **150**, 81–97 (2024).
37. Y. Liu, P. H. Daum, R. L. McGraw, M. A. Miller, S. Niu, *Geophys. Res. Lett.* **34**, L16821 (2007).
38. R. F. Cahalan, W. Ridgway, W. J. Wiscombe, T. L. Bell, J. B. Snider, *J. Atmos. Sci.* **51**, 2434–2455 (1994).
39. Z. Zhang *et al.*, *J. Geophys. Res.* **117**, D19208 (2012).
40. Y. Liu, P. H. Daum, *Geophys. Res. Lett.* **27**, 1903–1906 (2000).
41. Y. Liu, M.-K. Yau, S.-i. Shima, C. Lu, S. Chen, *Adv. Atmos. Sci.* **40**, 747–790 (2023).

ACKNOWLEDGMENTS

We thank A. Kostinski (Michigan Technological University) for early discussions that inspired the use of the Kolmogorov-Smirnov test and A. G. Shaw (Brigham Young University) for his contributions to developing the algorithm used in this study. We thank the staff of the ARM Aerial Facility for their role in obtaining the data during the ACE-ENA project and the team led by J. Wang (Washington University) for project leadership. We thank the staff of the NCAR Earth Observing Laboratory for helping to prepare the HOLODEC instrument for deployment. The High-Performance Computing Shared Facility (Superior) at Michigan Technological University was used in obtaining the results presented in this publication. We thank the anonymous reviewers for helping to improve the quality of the manuscript. **Funding:** This research was supported primarily by the US Department of Energy's Atmospheric System Research, an Office of Science Biological and Environmental Research program, under DE-SC0020053 (R.A.S.) and through the National Science Foundation awards AGS-2019649 (R.A.S.) and AGS-2001490 (M.L.L.). **Authors contributions:** N.A., M.L.L., and R.A.S. conceptualized and designed the research. S.G. and R.A.S. obtained the data. N.A. and S.G. processed the data. N.A. wrote the code to analyze the data. N.A., M.L.L., and R.A.S. performed analysis and wrote the paper. **Competing interests:** The authors declare that they have no competing interests. **Data and materials availability:** The HOLODEC data used in this study are available online (*25*).

SUPPLEMENTARY MATERIALS

science.org/doi/10.1126/science.adi5550
Materials and Methods
Supplementary Text
Figs. S1 to S3
Tables S1 and S2
References (*42*–*49*)

Submitted 5 May 2023; accepted 29 March 2024
10.1126/science.adi5550